

We are IntechOpen, the world's leading publisher of Open Access books Built by scientists, for scientists

6,900

Open access books available

185,000

International authors and editors

200M

Downloads

Our authors are among the

154

Countries delivered to

TOP 1%

most cited scientists

12.2%

Contributors from top 500 universities



WEB OF SCIENCE™

Selection of our books indexed in the Book Citation Index
in Web of Science™ Core Collection (BKCI)

Interested in publishing with us?
Contact book.department@intechopen.com

Numbers displayed above are based on latest data collected.
For more information visit www.intechopen.com



What Is Vibrational Raman Spectroscopy: A Vibrational or an Electronic Spectroscopic Technique or Both?

Søren Hassing

Abstract

Modern Raman spectroscopy covers several noninvasive reflection techniques for identification of molecules and investigation of molecular properties. All are based on the Raman effect, occurring when polarized laser light is inelastically scattered by a molecular sample. Vibrational Raman spectroscopy is the Raman technique most widely used in chemical analysis, and it is relevant for the characterization of molecules in solution, biomolecules, and solids (crystals and powders). In this chapter vibrational Raman spectroscopy is discussed under the headline: “What is vibrational Raman spectroscopy: a vibrational or an electronic spectroscopic technique, or both?” The answer to this question is gained through a discussion of different scattering situations, and it is demonstrated that the Raman technique is more than an alternative technique to infrared and near-infrared absorption spectroscopy. Starting with the Kramers-Heisenberg equation, the answer is obtained through a discussion of: State tensors and Raman tensors, non-resonance and resonance Raman scattering (RRS) excited with a single laser wavelength, and unpolarized and polarization-resolved RRS excited with variable laser wavelengths (RADIS), dispersive Raman vibrations as a tool for noninvasive detection of molecular color changes and that RADIS data are automatically born as three-dimensional multivariate data with high information contents.

Keywords: Raman, resonance Raman, RADIS, polarization dispersion, state tensor, Raman tensor, noninvasive

1. Introduction

Modern Raman spectroscopy is a class of well-documented, noninvasive, optical reflection techniques with a high spectral resolution applicable for the identification of molecules and investigation of molecular properties. All are based on the Raman effect, discovered by Raman in 1928 [1, 2]. Today more than 25 different Raman spectroscopic techniques are known [3]. The Raman effect occurs when light is inelastically scattered by a molecular sample.

Originally Raman and Krishnan observed the scattering of spectrally filtered sunlight from a liquid and found that the scattered light contained very weak

components of light, which had slightly different frequencies compared to the frequency of the incoming light. In a description of the scattering process based on quantum mechanics, the appearance of the shifted frequencies in the Raman scattered light is interpreted in the way that the molecules have shifted quantum state during the process. The shifted frequencies appear symmetrically around the frequency of the exciting light, from which one can conclude that the molecule may either be excited or de-excited during the scattering process. The last requires that the molecules have been excited (e.g., thermally) before the scattering event. This is termed anti-Stokes scattering, while the scattering where the molecules are excited during the process is termed Stokes scattering. The molecules may either shift rotational, vibrational, or electronic state during the scattering, depending on the molecule and the specific experimental conditions.

The spectroscopic technique based on Raman scattering, where the molecules shift vibrational state, is termed vibrational Raman spectroscopy. A vibrational Raman spectrum contains the unique and highly resolved vibrational signature of the scattering molecule. Normally only the Stokes part of the entire spectrum is measured, since this is more intense than the anti-Stokes part [3]. Vibrational Raman spectroscopy is the Raman technique most widely used in chemical analysis, and it is relevant for the investigation of molecules in solution, biomolecules, and solids (crystals and powders). Since the Raman technique can be performed as a reflection measurement, which requires no or very little sample preparation, it is well suited for the investigation of molecules in their natural environment such as in the food industry and in medical and environmental applications.

Nowadays vibrational Raman spectra are measured by illuminating the sample with polarized laser light with wave numbers either in the near-infrared (NIR), the visible (VIS), or the ultraviolet (UV) and simultaneously monitoring the reflected light. A vibrational Raman spectrum is then obtained by considering the intensity distribution in the Raman scattered light as a function of the so-called Raman shift $\Delta\tilde{\nu}_R$ defined as $\Delta\tilde{\nu}_R = \tilde{\nu}_{laser} - \tilde{\nu}_s$, where $\tilde{\nu}_s$ and $\tilde{\nu}_{laser}$ are the wave numbers of the Raman scattered light and the laser, respectively. In the case of Stokes scattering, $\Delta\tilde{\nu}_R$ is positive.

Ever since the discovery of the Raman effect in 1928, the Achilles heel of Raman spectroscopy has been the low Raman cross section where typically 10^8 incoming photons only generate a single Raman photon. The consequence is that the intensity of the Raman signal becomes very low in general. In the history of Raman spectroscopy, many attempts have been made to overcome this disadvantage. The three most important milestones for the practical application of Raman spectroscopy are the following:

- The invention and development of commercial lasers [4, 5]
- The development of sensitive charge-coupled devices (CCD-detectors) [6, 7]
- The development of interference filters, i.e., notch and edge filters

Not before the implementation of these three improvements could Raman spectroscopy really compete with the competing spectroscopic techniques IR, NIR, and UV/VIS.

A challenge particular in in situ resonance Raman investigations of biomolecules is that the excitation of the resonance Raman process is followed by a simultaneous excitation of fluorescence in either the molecule under investigation or in other molecules present in the sample. Since in general the fluorescence cross section is

much larger than the Raman cross section, the Raman peaks typically ride on top of the spectrally broad fluorescence background so that it can be time-consuming to determine the true Raman intensity. Sometimes a part of the Raman spectrum may even be hidden behind the fluorescence. However, in most situations the influence from fluorescence may be taken care of by changing the laser wave number to NIR or to UV, by applying a fluorescence quenching technique [8], by applying a pulsed detection technique, or by implementing advanced signal processing including multivariate analysis.

In the present chapter vibrational Raman spectroscopy is discussed under the headline: “What is vibrational Raman spectroscopy: a vibrational or an electronic spectroscopic technique, or both?” Besides giving an answer to this question, the goal of the chapter is twofold: (1) to improve the readers’ understanding of Raman scattering in general and (2) to demonstrate which kind of molecular information one may achieve by choosing different experimental conditions.

Before we begin the discussion, it should be noticed that Raman spectroscopy, like any kind of molecular spectroscopy, can be applied in two different ways: (1) as an analytical technique for the identification and quantification of molecules in a sample and (2) as a technique for studying the physical and chemical properties of molecules. In the first kind of application, the Raman signal is just considered as a source of data, which has to be compared with spectroscopic databases or which has to be combined with the chemometric method being most appropriate for the problem to be solved. For this kind of application, no knowledge of Raman theory and how the theory is applied to molecules is really needed. But it should be noticed that to decide how the chemometrics should be applied together with the Raman data, one must take into account that vibrational Raman spectra are in general characterized by exhibiting high spectral resolution (narrow and well-separated lines) compared to the broader bands typically found in IR and in particular in UV/VIS spectra. For the second kind of applications, a deeper understanding of molecular physics and molecular Raman theory is needed.

2. Some fundamentals of Raman theory

2.1 General theory

A unified treatment of Raman theory can be found in [9, 10] and in [3], where in the last reference a long list of references to the Raman literature is provided. The symmetry aspects, interference phenomena, and polarization properties of resonance Raman scattering have been discussed by Mortensen and Hassing [11] and by Schweitzer-Stenner [12], while the vibronic aspects has been discussed by Siebrand and Zgierski [13].

Raman scattering can be described as a coherent absorption-emission sequence in which a primary photon with wave number $\tilde{\nu}_p$ and polarization vector u_p is replaced by a scattered photon with wave number $\tilde{\nu}_s$ and polarization vector u_s . In comparison, fluorescence is an incoherent absorption-emission sequence, i.e., a combination of two independent processes, namely, a real absorption of a primary photon followed by a spontaneous emission of a secondary photon. In fluorescence the initially excited molecule is allowed to decay into other quantum states before the spontaneous emission of light. As well known, the number of vibrations in a molecule is given by the expression $3N - 6$, where N is the number of atoms in the molecule. Since each vibration can be highly excited, it follows that the total number of vibrational states associated with every electronic state including the

electronic ground state increases strongly with the size of the molecule. This gives many possibilities for the decay and accordingly also for the emission of the light. When the intensity contributions from all the possible radiative transitions are superposed to give the total intensity, the individual spectra overlap with the result that the spectral distribution of the fluorescence becomes broad and without much structure. In contrast, the number of accessible final states in the Raman process is very limited due to the coherent nature of the process. The typical vibrational Raman spectrum consists of narrow Raman lines with the typical FWHM bandwidths of $10\text{--}20\text{ cm}^{-1}$.

The basic equation for the theoretical description of Raman scattering is the famous Kramers-Heisenberg (KH) dispersion relation. Kramers and Heisenberg derived the equation by the application of the correspondence principle to the classical dispersion relation. The KH equation expresses the transition probability per second for Raman scattering [14]. The original version did not contain the damping of the scattering system, and thus it did not immediately apply to resonance Raman scattering. Later Weisskopf modified the equation by introducing the damping of the atomic and molecular states with the assumption of an exponential decay of the excited states [15]. Within a modern theoretical framework, the KH relation and the expression for the intensity of the Raman scattered light can be derived by using formal scattering theory [16] or time-dependent second-order perturbation theory. In perturbation theory the interaction energy between the molecule and radiation field, normally considered in the electric dipole approximation, is used as the perturbation, when the time-dependent Schrödinger equation for the total system and molecule plus electromagnetic field is solved (e.g., see [17]).

The basic scattering equations are collected in Eq. (1). The transition probability is expressed through the total differential scattering cross section $\left(\frac{d\sigma}{d\Omega}\right) = \frac{I_{\text{Raman}}}{I_{\text{laser}}}$. Since the intensity of the laser I_{laser} refers to a plane wave and the intensity of the Raman scattered light I_{Raman} is the intensity scattered into the solid angle $d\Omega$, the scattering cross section $\left(\frac{d\sigma}{d\Omega}\right)$ becomes an area. It follows from Eq. (1) that the intensity of the Raman scattered light corresponding to the Raman transition $|a\rangle \rightarrow |b\rangle$ is proportional to the intensity of the laser I_{laser} and to the absolute square of the Raman tensor, $|\alpha^{a \rightarrow b}|^2$, where $\alpha^{a \rightarrow b}$ is a tensor of rank 2 represented by a 3×3 matrix, which is related to the electric polarizability of the molecule. The expression for the Cartesian components of the Raman tensor $\alpha_{\rho\sigma}^{a \rightarrow b}$ ($\rho\sigma = x, y, z$) is also given in Eq. (1):

$$I_{\text{Raman}} = \left(\frac{d\sigma}{d\Omega}\right) I_{\text{laser}} d\Omega$$

$$\left(\frac{d\sigma}{d\Omega}\right) = 4\pi\alpha_{\text{fsc}}^2 \tilde{\nu}_s^4 \left| \sum_{\rho\sigma} u_{s\rho} \alpha_{\rho\sigma}^{a \rightarrow b} u_{p\sigma} \right|^2 \quad (1)$$

$$\alpha_{\rho\sigma}^{a \rightarrow b} = \sum_r \frac{\langle b|\rho|r\rangle \langle r|\sigma|a\rangle}{\tilde{\nu}_{r,a} - \tilde{\nu}_p - i\gamma_r} + \frac{\langle b|\sigma|r\rangle \langle r|\rho|a\rangle}{\tilde{\nu}_{r,b} + \tilde{\nu}_p + i\gamma_r}$$

α_{fsc} is the fine structure constant known from atomic physics [17]. Notice that the Raman intensity is proportional to the fourth power of the wave number of the scattered light (i.e., inversely proportional to the fourth power of the wavelength). This means that the intensity of a Raman spectrum measured with a NIR laser with wavelength 1064 nm is decreased with a factor of 16 relative to the intensity of the same spectrum measured with a visible laser with wavelength 532 nm.

In the expression for the Raman tensor in Eq. (1), $|a\rangle$, $|b\rangle$ and $|r\rangle$ is the initial, the final, and the intermediate states of the molecule. In principle, all states are exact eigenstates of the molecular Hamiltonian. ρ , σ is a shorthand notation for the Cartesian components of the electric dipole moment of the molecule divided by the velocity of light and measured relative to a coordinate system in the center of mass of the molecule. $\tilde{\nu}_{r,a}$ is the wave number difference between the states $|r\rangle$ and $|a\rangle$. γ_r is the damping of the state $|r\rangle$ given as the FWHM width and represents the exponential decay of the state. The matrix elements in the numerators of the two terms in the Raman tensor are given in the Dirac notation [18] and involve mathematically an integration over the coordinates used in the functions describing the molecular states. The terms in the expression for the Raman tensor, where the denominators contain the wave number difference between the state $|r\rangle$ and the laser $\tilde{\nu}_p$, are called the resonance terms, since their contributions to the Raman intensity increase strongly when the excitation wave number $\tilde{\nu}_p$ becomes equal to their energies $\tilde{\nu}_{r,a}$. When this happens the scattering process is called resonance Raman scattering (RRS), while in cases where $\tilde{\nu}_p \ll \tilde{\nu}_{r,a}$, the process is just called Raman scattering (RS). The difference between RRS and RS and the implications with respect to the kind of molecular information one may obtain in the two scattering situations will be discussed in more detail in the following.

It follows from Eq. (1) that all the molecular states contribute to the intensity of the specific Raman transition $|a\rangle \rightarrow |b\rangle$. It also follows that the first step in the calculation of the intensity is to calculate the Raman tensor by performing the summation over all molecular states and then as the second step calculate the absolute square of the result. The consequence is that the contribution from each state will interfere either constructively or destructively with the contributions from all other states in the Raman intensity. The interference between the individual contributions depends on their magnitude and relative sign. An important issue in the evaluation of the expression for the Raman intensity is to establish the relations between the molecular properties and the Raman process. To achieve this goal, it is appropriate to divide the discussion into two parts: (1) discussion of the contribution to the scattering tensor from a single state and (2) discussion of the interference between the contributions from different states. For that purpose Mortensen and Hassing [11] defined the state tensor $S_{\rho\sigma}^{(r)}$ corresponding to the intermediate state $|r\rangle$:

$$S_{\rho\sigma}^{(r)} \equiv \langle b|\rho|r\rangle \langle r|\sigma|a\rangle \quad (2)$$

The state tensor determines the contribution to the scattering from that particular state. $S_{\rho\sigma}^{(r)}$ depends also on the initial and final states of the Raman process $|a\rangle$ and $|b\rangle$, but we omit these indices for simplicity in writing.

The Raman tensor now becomes

$$\alpha_{\rho\sigma}^{a \rightarrow b} = \sum_r \frac{S_{\rho\sigma}^{(r)}}{\tilde{\nu}_{r,a} - \tilde{\nu}_p - i\gamma_r} + \frac{S_{\sigma\rho}^{(r)}}{\tilde{\nu}_{r,b} + \tilde{\nu}_p + i\gamma_r} \quad (3)$$

The introduction of the state tensor is more important in RRS, where only relative few states contribute significantly to the Raman intensity than in RS, where all molecular states contribute with the result that the information of their individual contributions is blurred.

One advantage of introducing the state tensor is that it is possible to evaluate the general form of the state tensor in cases, where the symmetry of the molecule is

known. First, we notice that when the molecule has no symmetry, the state tensors are determined exclusively by the physical properties of the specific molecule considered, and all state tensor components may a priori be nonvanishing. The same holds for the Raman tensor, since it is a superposition of state tensors scaled with the associated energy factors. However, when the molecule exhibits some symmetry, the state tensors will be determined both by the physics and by the constraints imposed by the symmetry. The consequence of the symmetry is that some tensor components vanish. When the symmetry gets higher, the number of vanishing state tensor components increases. It is also important to notice that the structure of each state tensor contributing to a specific Raman transition can be different and different from the structure of the Raman tensor. This is because the state tensors are determined by the symmetry and the physical properties of the individual states, which contribute to the scattering, while the Raman tensor is a superposition of the state tensors. As we shall see later, this is particularly important in resonance Raman scattering of molecules containing a chromophore with high symmetry such as the molecules containing the heme group.

Traditionally the symmetry of a molecule with well-defined configuration has been described by using point groups and group representation theory, and from the early days of quantum physics, this has been used to derive selection rules, i.e., to give the conditions under which a particular matrix element must vanish. In spectroscopy the symmetry-based selection rules determine when a transition does not appear in the spectrum, i.e., it is a symmetry-forbidden transition.

In cases where the molecular point group has a threefold rotation axis or axes of higher order, one must, however, as demonstrated in [11] and by Mortensen in [19], apply the so-called non-commuting generator (NCG) approach to molecular symmetry in order to be able to evaluate the general form of the state tensors. In [19] the NCG approach is explained in detail, while in [11] it is shown how the method can be applied to calculate the structure of the state tensors both for molecules with integer and half integer spin. Besides all the possible state tensors for molecules with integer spin in the most important point groups have been evaluated and collected as an appendix. The appendix containing the state tensors is also reproduced in [3].

Recently [20] the NCG method has been extended and applied to develop the state and Raman tensors for molecular aggregates. Specifically the tensors for the H-type dimer of two coupled monomers with D_{4h} symmetry are evaluated, and the result has been applied to interpret the experimental results of polarized resolved RRS spectra of a diluted solution of red blood cells (RBCs) of human blood. The main conclusion from this study is that aggregation between heme-protein molecules inside the RBC can be studied in vivo by polarized RRS, which opens the possibility of monitoring the effects on the aggregation of drugs added to the blood.

2.2 Polarization properties of Raman scattering

The polarization is a unique property of Raman scattering, which distinguishes the Raman technique from the UV/VIS and IR spectroscopy. In general, the polarization of the Raman scattered light is different from the polarization of the incoming laser light. This property is valid for oriented molecules (crystals), but perhaps more surprisingly, it is also valid for randomly oriented molecules like molecules in solutions and in powders. The reason for this is that the Raman process is controlled by a tensor (the Raman tensor) and not by a vector (the electric dipole vector) like in UV/VIS and IR absorption. While a vector only has one quantity, namely, its length, which is not changed (invariant) under rotation of the molecules, a tensor of rank 2 has three combinations of the nine tensor components, which are invariant

to rotation. In the Raman case, these are called the rotational invariants of the Raman tensor, and they are denoted as Σ^0 , Σ^1 , and Σ^2 . Recently the polarization properties of resonance Raman have been discussed in [20]. It is demonstrated that the amount of molecular information, which may be extracted from a resonance Raman experiment, can be increased considerably by measuring the polarization-resolved Raman signals in addition to the unpolarized signals. Specifically the results of two case studies are discussed. As already mentioned the first focuses on the aggregation of hemoglobin inside RBCs of human blood, and the second is an in vitro study of the stability of dye-sensitized solar cells. Here we shall only define the polarization properties relevant for the discussion that follows below, and we refer to [11, 20] for further details.

In polarization-resolved Raman experiments, two spectra are measured from which the parallel $(\frac{d\sigma}{d\Omega})_{\parallel}$ and perpendicular $(\frac{d\sigma}{d\Omega})_{\perp}$ scattering cross sections can be determined by using the relation in Eq. (1).

The polarization properties in Raman scattering are expressed through the depolarization ratio (DPR) defined as

$$DPR \equiv \frac{(\frac{d\sigma}{d\Omega})_{\perp}}{(\frac{d\sigma}{d\Omega})_{\parallel}} \quad (4)$$

The polarization-resolved Raman measurements are illustrated in **Figure 1**, which shows the 180° scattering geometry (reflection measurement) being the geometry mostly used. The molecule (M) is placed in the center of a space-fixed coordinate system, and the laser light, which is linearly polarized along the Z – axis, is propagating along the X – axis in the negative direction. The Raman signals back reflected from the molecule are measured with a detector placed on the X – axis and with the polarization analyzers directed along the Z – axis for measurement of the parallel component $|\alpha_{ZZ}^{a \rightarrow b}|^2$ (marked red in **Figure 1**) and along the Y – axis for

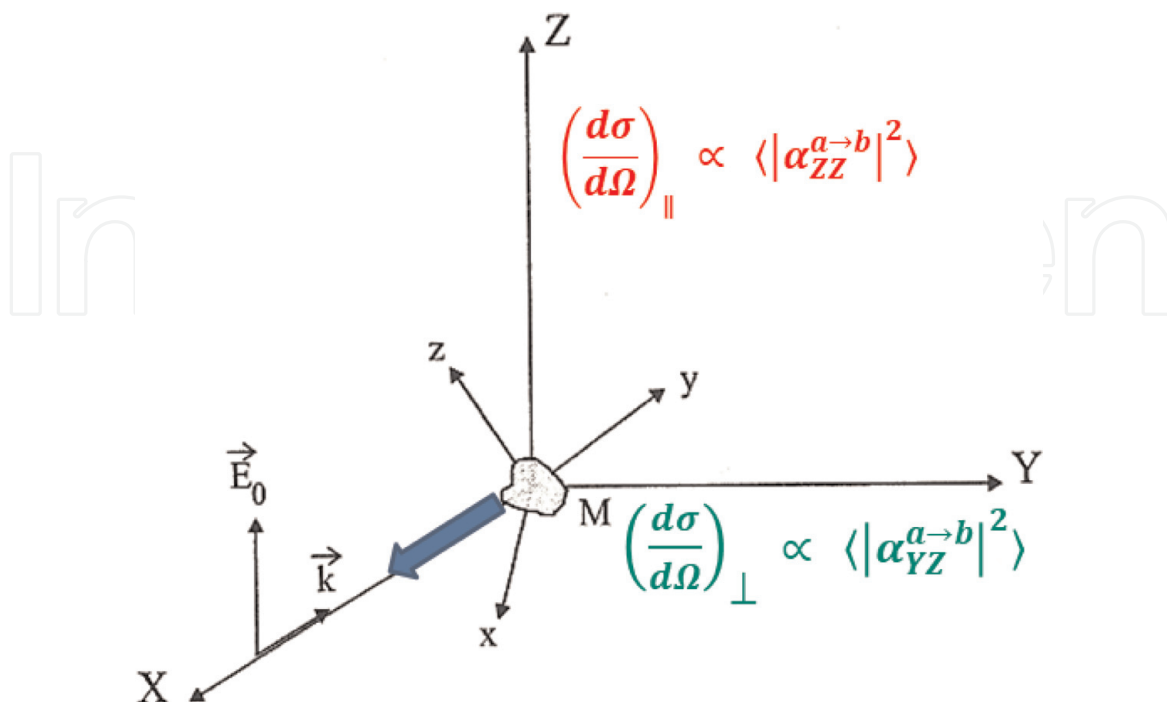


Figure 1.
 Backscattering geometry illustrating polarized resolved Raman measurements of the parallel (along Z) and perpendicular (along Y) polarized data. \vec{E}_0 and \vec{k} are the polarization and k -vector of the laser. M is the randomly oriented molecule.

measurement of the perpendicular polarized component $|\alpha_{YZ}^{a \rightarrow b}|^2$ (marked green in **Figure 1**). For randomly oriented molecules, i.e., solutions and powders, we have to perform an average calculation of these scattering quantities with respect to orientation of the molecule. The average quantities $\langle |\alpha_{ZZ}^{a \rightarrow b}|^2 \rangle$ and $\langle |\alpha_{YZ}^{a \rightarrow b}|^2 \rangle$ have been calculated in [11] by the application of angular momentum theory, and we refer to [11] for details. The result for the DPR is as follows:

$$DPR = \frac{\langle |\alpha_{YZ}^{a \rightarrow b}|^2 \rangle}{\langle |\alpha_{ZZ}^{a \rightarrow b}|^2 \rangle} = \frac{5\Sigma^1 + 3\Sigma^2}{10\Sigma^0 + 4\Sigma^2} \quad (5)$$

where Σ^0 , Σ^1 , and Σ^2 are the rotational invariants mentioned above and each of them is a combination of the absolute squares of the Raman tensor components given in molecule-fixed coordinates [11]. Σ^0 is the absolute square of the trace of the tensor, Σ^2 is the symmetric anisotropy, and Σ^1 refers to the antisymmetric part of the Raman tensor, i.e., it contains terms of the form $|\alpha_{\rho\sigma}^{a \rightarrow b} - \alpha_{\sigma\rho}^{a \rightarrow b}|^2$.

2.3 Vibronic expansion of the state and Raman tensors

From the beginning of the history of Raman spectroscopy, it has been an important task to transform the basic and general scattering expressions into a form suitable for the interpretation of experimental Raman data. It follows from Eq. (1) that an important problem is that the calculation of the Raman intensity involves a summation over all molecular states, which are not known. Another problem is that in a molecule, the motions of the electrons and nuclei are not independent, which means that the functions describing the molecular states depend upon coordinates defining the positions of both the electrons and nuclei. It follows that any evaluation of the expression for the Raman intensity requires the introduction of approximations. It seems that there exist two different kinds of approach: the first approach introduces a number of radical approximations in one step, which leads to simple results, but with limited applicability. This approach was first followed by Placzek in 1934 with the development of his polarizability theory, which is valid for non-resonance Raman scattering [9]. The polarizability theory has been reconsidered by Long in 2002 [3] and is also briefly discussed below. The second approach introduces a number of approximations in a stepwise way directed toward Raman scattering in specific molecular systems. This kind of approach became relevant after the invention of the laser and development of commercial lasers, in particular tunable lasers in the 1960s and 1970s by which it became possible to perform resonance Raman experiments where the wave number of the laser was scanned through the visible absorption band of a large molecule. In particular, resonance Raman studies of biological molecules containing a chromophore came into focus [21–24]. Accordingly, it became necessary to transform the basic equations into a form suitable for the interpretation and extraction of the molecular information obtained under resonance conditions.

Almost all theoretical treatments of optical spectroscopic processes in molecules, including UV/VIS and Raman spectroscopy, are formulated within the adiabatic formalism. This formalism is based upon the assumption that in a molecule the motions of the light electrons are only weakly correlated to the motions of the heavy nuclei, so that it is possible to approximately separate these motions, when the Schrödinger equation for the molecule is solved. In this chapter we focus on

vibrational Raman spectroscopy of larger molecules, i.e., either crystals or solutions and powders. In these molecules, the rotational spectra are not resolved, which means that it is not necessary to consider the rotational motion explicitly. In the adiabatic Born-Oppenheimer (ABO) approximation (e.g., see [17]), each molecular eigenstate is therefore, as a first step, approximated by a product of an electronic state and a vibrational state, where the latter is normally considered within the harmonic approximation. Within the ABO approximation, the states in the state and Raman tensors are replaced by the product states: $|a\rangle = |g\rangle|v_a\rangle$, $|b\rangle = |g\rangle|v_b\rangle$ and $|r\rangle = |e\rangle|v_e\rangle$ where g and e are the electronic ground state and an excited electronic state, respectively. $|v_e\rangle = |v_1, v_2, v_3, v_4, \dots, v_{3N-6}\rangle$ is the vibrational sub-state associated with the electronic state e , where in the harmonic approximation the vibrational state is also factorized in the product of $3N - 6$, and one-dimensional harmonic oscillator states, each of which describing a normal vibration. N is the number of atoms in the molecule. However there are situations where the ABO approximation breaks down the product functions that serve in general as good approximations to the molecular wavefunctions. The most important situation for resonance Raman scattering, where it is necessary to go beyond the ABO approximation, is the one where an excited electronic state is coupled to the high-lying vibrational states belonging to the electronic ground state. The nonadiabatic coupling is mainly provided by the \hat{T}_N - operator, which is the operator describing the kinetic energy of the nuclei. This gives rise to radiationless transitions, which leads to an increase of the damping constant of the excited electronic state and explains essentially why the magnitude of the bandwidths observed in experimental UV/VIS absorption spectra is larger than the radiation damping. For the discussion given here, it is sufficient to associate the bandwidths estimated in UV/VIS spectra with the constant $\gamma_{r=ev}$ used in the Raman tensor. See [25, 26] for further discussions of the origin of the bandwidths found in Raman and UV/VIS experiments.

Since the ABO approximation only allows a partial separation of the electronic and nuclear motions, the functions describing the electronic states will depend on both the electronic coordinates and on the nuclear coordinates, while the vibrational functions only depend on the nuclear coordinates. However, the vibrational motion depends indirectly on the electronic state, since the electronic eigenvalue is a function of the nuclear coordinates and is found to play the role of the potential energy function for the vibrational motion.

The vibronic version of the state tensor in Eq. (2) may now be written as

$$S_{\rho\sigma}^{[e]|v_e\rangle} = \langle g(q, Q)|v_b(Q)|\rho(q)|e(q, Q)|v_e(Q)\rangle \langle e(q, Q)|v_e(Q)|\sigma(q)|g(q, Q)|v_a(Q)\rangle \quad (6)$$

where q and Q symbolize the set of electronic and nuclear position coordinates, respectively. Thus each of the two matrix elements in the state tensor is evaluated by integrating formally over both the electronic and the nuclear coordinates. Besides, according to the adiabatic idea, the integration over the electronic coordinates should be performed before the integration over the nuclear coordinates.

In general, the functions describing the excited electronic states in larger molecules are not known. In fact, one important task in optical spectroscopy is to provide knowledge of these functions. Since also their dependence on the nuclear coordinates is not known, the formal integrations over the nuclear coordinates in the state tensor given in Eq. (6) are performed by introducing an appropriate Taylor expansion in the nuclear coordinates. The expansion of the state tensors may be performed in two different ways: (1) the electronic functions are expanded using perturbation theory and then the integration over the nuclear coordinates are performed (e.g., see [27]), and (2) the electronic transition moments $\rho(Q) = \langle g(q, Q)|\rho(q)|e(q, Q)\rangle$ and $\sigma_{eg}(Q) = \langle e(q, Q)|\sigma(q)|g(q, Q)\rangle$ defined through

the formal integration over the electronic coordinates are Taylor expanded in the nuclear coordinates (e.g., see [11]). After the expansion of the state tensors in Eq. (6), using either scheme 1 or 2, the result is inserted in Eq. (1) in order to obtain the Raman intensity. Applying (2) to the first order (being in most cases sufficient), the state tensor in Eq. (6) becomes

$$S_{\rho\sigma}^{[e]|v_e\rangle} = \langle v_b|v_e\rangle \langle v_e|v_a\rangle \rho_{ge}^0 \sigma_{eg}^0 + \sum_{k=1}^{3N-6} \langle v_b|Q_k|v_e\rangle \langle v_e|v_a\rangle \left(\frac{\partial \rho_{ge}}{\partial Q_k} \right)_0 \sigma_{eg}^0 + \langle v_b|v_e\rangle \langle v_e|Q_k|v_a\rangle \rho_{ge}^0 \left(\frac{\partial \sigma_{eg}}{\partial Q_k} \right)_0 \quad (7)$$

where all vibrational states are functions of the set of normal coordinate Q . The first and second lines are the state tensor in the Franck-Condon and the Herzberg-Teller approximations, respectively. Comparing Eq. (7) with the result in [27], it follows that the second expansion scheme leads to the simplest parametrization of the expression for the Raman intensity; although taken to infinite order, which is of course impossible in practice, the two expansion schemes are equivalent.

The vibronic models developed for RRS, which are found in the Raman literature, differ essentially from each other in two ways: (1) whether expansion scheme 1 or 2 has been applied and (2) the degree of approximation that has been introduced.

3. What is vibrational Raman spectroscopy: a vibrational or an electronic spectroscopic technique or both?

3.1 Non-resonance Raman spectroscopy

In most molecules, the energy differences between the electronic ground state and the excited electronic states are much larger than the mutual energy difference between the excited electronic states. Typically, there will therefore exist a relatively large spectral region between the energy of the final state in the Raman process and the energy of the first electronically excited state, where the wave number of the laser $\tilde{\nu}_p$ can be chosen without exciting an electronic absorption. Besides, $\tilde{\nu}_p$ will also typically be much larger than molecular vibrational frequencies, so that all the terms in the Raman tensor in Eq. (1) where r runs over vibrational quantum numbers in the electronic ground state can be neglected relative to the contributions which involves excited electronic states, i.e., $\Delta\tilde{\nu}_R = \tilde{\nu}_{v_b, v_a} \ll \tilde{\nu}_p \ll \tilde{\nu}_{ev, gv_a}$. The damping constant of the excited electronic states $\gamma_{r=e}$ may also be neglected since they are of the order of magnitude as a vibrational quantum. With these assumptions and assuming that the electronic ground state is nondegenerate (which is typical), the expression for the Raman tensor in Eq. (1) can be approximated by

$$\left(\alpha_{\rho\sigma}^{v_a \rightarrow v_b} \right)_{non-res} \cong \left\langle v_b | \hat{\alpha}_{\rho\sigma} \left(Q, \tilde{\nu}_{v_b, v_a}, \tilde{\nu}_p \right) | v_a \right\rangle \quad (8)$$

where $\hat{\alpha}_{\rho\sigma} \left(Q, \tilde{\nu}_{v_b, v_a}, \tilde{\nu}_p \right)$ is the Cartesian component of the molecular transition polarizability tensor

$$\hat{\alpha}_{\rho\sigma}(Q, \tilde{\nu}_{v_b, v_a}, \tilde{\nu}_p) = \sum_{e \neq g} \frac{\rho_{ge}(Q) \sigma_{eg}(Q)}{\tilde{\nu}_{e,g} - \tilde{\nu}_p} + \frac{\sigma_{ge}(Q) \rho_{eg}(Q)}{\tilde{\nu}_{e,g} + \tilde{\nu}_p} \quad (9)$$

To obtain Eq. (9) “the closure rule,” i.e., $\hat{1} = \sum_i |i\rangle \langle i|$ valid for any complete set of states $|i\rangle$, has been applied to the vibrational sub-states of every electronic state, and the electronic transition moments defined above (expansion scheme 2) have been introduced. Because Eq. (9) involves a summation over all excited electronic states, a Taylor expansion of the electronic transition moments $\rho_{ge}(Q)$ and $\sigma_{eg}(Q)$ would result in too many parameters, which cannot be determined. A direct Taylor expansion of the molecular transition polarizability tensor $\hat{\alpha}_{\rho\sigma}(Q, \tilde{\nu}_{v_b, v_a}, \tilde{\nu}_p)$ is therefore more convenient in this case:

$$\hat{\alpha}_{\rho\sigma}(Q, \tilde{\nu}_{v_b, v_a}, \tilde{\nu}_p) \cong \hat{\alpha}_{\rho\sigma}^0 + \sum_{k=1}^{3N-6} \left(\frac{\partial \hat{\alpha}_{\rho\sigma}}{\partial Q_k} \right)_0 Q_k + \dots \quad (10)$$

where Q_k is the k^{th} normal coordinate. To calculate the Raman tensor, the expansion in Eq. (10) is inserted in Eq. (8), and the result is inserted in Eq. (1) in order to obtain the intensity of the Raman signal of the Raman transition $|a\rangle \rightarrow |b\rangle$.

Conclusion: It follows that the Raman signal only depends on variables related to the electronic ground state, i.e., the set of normal coordinates Q and the wave numbers of the Raman bands $\tilde{\nu}_{v_b, v_a}$, besides the wave number of the laser $\tilde{\nu}_p$. However, the spectral distribution in the Raman spectra is independent of the laser wave number, which only has influence on the absolute intensity of the Raman signal. As seen from Eq. (9), all information about the individual electronically excited states is “washed out” in the calculation (and in the experimental signals), which means that we cannot obtain any information on individual excited electronic states by measuring the Raman signals under these conditions. Non-resonance Raman scattering (or RS for short) becomes therefore a vibrational spectroscopic technique just like IR and NIR. There are however two essential differences between RS and IR and NIR: first, the Raman signals are obtained by the scattering of laser light with wave numbers typically in the visible region and therefore much higher than the wave numbers of the IR and NIR photons, which are directly absorbed in IR and NIR spectroscopy. Second, since the Raman signal is controlled by a tensor instead of by a vector, the spectral selection rules of RS become different from those of IR and NIR. The selection rules for RS can easily be derived by considering Eq. (10) inserted in Eq. (8). Assuming room temperature and considering only the Stokes spectrum, it follows that Raman spectra only contain the fundamental transitions, i.e., $|v_a = 0\rangle \rightarrow |v_b = 1\rangle$, where the intensity is provided by the first derivative of the polarizability tensor. Besides for smaller molecules (e.g., benzene) having a high symmetry, the polarization enables one to distinguish between totally symmetric and asymmetric vibrations in the Raman spectrum. The DPR for symmetric vibrations becomes $0 \leq DPR < 0.75$, which follows directly from Eq. (5) and the fact that the Raman tensor is symmetric in non-resonance (i.e., $\Sigma^1 = 0$). For asymmetric vibrations the $DPR = 0.75$, since the tensor, because of the symmetry, has no trace (i.e., $\Sigma^0 = 0$) for these modes. For molecules without symmetry, all vibrations are of course in principle totally symmetric. Due to the generally narrow bandwidths of the Raman bands, Raman spectra represent in most cases a very well-defined vibrational signature of the molecule. For this reason and since the Raman signal can be measured in a reflection geometry and because no sample preparation is really needed, Raman signals are

well suited for performing different kinds of multivariate analysis of solutions containing several molecular species.

3.2 Vibrational resonance Raman spectroscopy

In resonance Raman scattering, the wave number of the laser is chosen within the UV or visible absorption band of the molecule. Since the assumption $\tilde{\nu}_{v_b, v_a} \ll \tilde{\nu}_p \ll \tilde{\nu}_{ev, gv_a}$ is no longer valid, we have to go back to Eqs. (3) and (8) and insert approximations appropriate for the resonant scattering situation to be considered. First it should be noticed that resonance Raman scattering may form the basis of two different kinds of resonance Raman spectroscopy:

1. Vibrational resonance Raman spectroscopy (VRRS)
2. Raman dispersion spectroscopy (RADIS) (see Section 3.3.)

In VRRS the vibrational Raman spectrum is measured in the same way as in RS, i.e., the spectral distribution in the Raman scattered light is measured as a function of the Raman shift $\Delta\tilde{\nu}_R$ with a **fixed value** of the wave number of the laser, but, as said, $\tilde{\nu}_p$ is now chosen close to or within an electronic absorption of the molecule. The two most striking features of VRRS as compared to RS are that the intensity of the Raman signal is largely enhanced (typically with a factor of $10^3 - 10^6$) and that the intensity distribution in the vibrational spectrum is different in general. It follows from Eq. (3) that the enhancement is due to the fact that the real part in the denominators of the Raman tensor becomes small or even zero for the states being close to or in resonance with the laser. Since the state tensors associated with the resonating states dominate in the Raman intensity, the selection rules will now be determined not only by the initial and final states as in the RS but also by these state tensors. It follows from Eq. (7) that this will change the intensity distribution of the Raman signal. A further consequence is that new vibrational modes may become Raman active, but more importantly not only the fundamentals are seen in VRRS spectra, but also overtones (i.e., multiple excitations of a single normal vibration) and combination bands (i.e., multiple excitations involving several vibrations) are frequently observed. The appearance of the overtones and combination bands enables one to estimate anharmonicity constants and thereby improve the modeling of the vibrational potential function in the electronic ground state.

Larger molecules, typically biomolecules, are often colored because they contain a chromophore with high symmetry. Important examples are the metal-porphyrins, where the ring structure has the ideal symmetry of D_{4h} . When the wave number of the laser is chosen within the visible absorption band of the chromophore, essentially only the ring vibrations are resonance enhanced and show up in the Raman spectra with significant intensity. Besides making the total Raman spectrum simpler, it also enables one to study a small part of a very large molecule, e.g., a protein molecule. Finally, it should be noticed that under resonance conditions, the value of the DPR may take any number from zero to infinity. This is because the Raman tensor needs no longer be symmetric but in general may have all three tensor invariants Σ^0 , Σ^1 , and Σ^2 different from zero. As seen from Eq. (5), the value infinity is obtained when the tensor is purely antisymmetric, i.e., when only $\Sigma^1 \neq 0$. In the 1970s very high values of the DPR of vibrational modes were first observed experimentally in the VRRS spectra of the heme-proteins [21]. The results were interpreted as being due to the scattering by a vibration with the symmetry a_{2g}

being associated with an antisymmetric state tensor for a resonating electronic state with E_u symmetry in the point group D_{4h} .

The resonance enhancement and the interference between the resonating state tensors are very sensitive to the magnitude of the damping constants $\gamma_{r=ev}$ of the resonating states. Since the damping is a measure of the lifetime of an excited electronic state, resonance Raman scattering may provide information about the dynamics of excited molecular states. However, to obtain this kind of information, measurement of the Raman signal at more than one laser wave number is required.

3.3 Raman dispersion spectroscopy (RADIS)

In RADIS the resonance Raman signal is monitored as a function of the excitation wave number. In practice a series of resonance Raman spectra are measured using either a number of discrete laser wave numbers or a tunable laser. RS, VRRS, and RADIS are illustrated in **Figure 2**. The figure illustrates, for a thought molecule, the changes in a series of Raman spectra obtained with increasing wave number toward resonance with an electronic state. The electronic resonance is illustrated by the UV/VIS absorption spectrum. One excitation spectrum, normally called an excitation profile (dotted curve), is obtained by plotting the intensity of a specific Raman band in the Raman spectrum versus the excitation wave number. It follows from the figure that there will be one excitation profile for each Raman band. It should be stressed that a complete RADIS experiment requires that two spectra are measured at each excitation wave number, namely, the parallel and perpendicular polarized spectra. From the polarized resolved spectra, the excitation profile can be calculated as the sum of these, but more importantly the DPR as a function of the excitation wave number can be determined. The DPR versus excitation wave number is called the polarization dispersion curve.

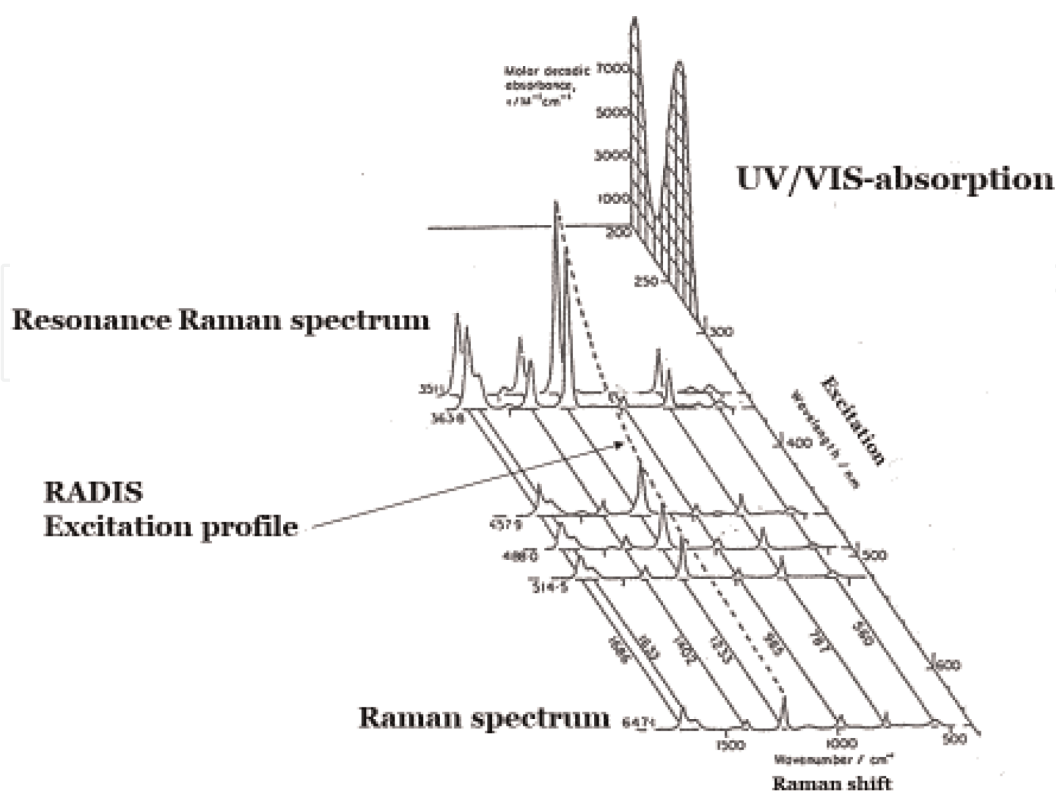


Figure 2.
 Illustration of Raman, resonance Raman, and Raman dispersion (RADIS) spectroscopy.

In a typical UV/VIS absorption experiment performed on a solution, one measures the absorbance A , which is related to the molar extinction coefficient $\varepsilon(\tilde{\nu})$ via Lambert-Beers law, $A = \varepsilon(\tilde{\nu})C_m l$, where C_m and l are the molar concentration and the path length, respectively. From the application of the quantum theory, the molar extinction coefficient is found to be proportional to the spatial average of the absolute square of the transition dipole moment:

$$\varepsilon(\tilde{\nu}) \propto \sum_{v_1^e, v_2^e, v_3^e \dots v_{3N-6}^e} \left| \left\langle v_1^e, v_2^e, v_3^e \dots v_{3N-6}^e | \rho_{ge}(Q) | 0, 0, 0, \dots \right\rangle \right|_{av}^2 L_i(\tilde{\nu}) \quad (11)$$

where $v_e \equiv v_1^e, v_2^e, v_3^e \dots v_{3N-6}^e$ are the vibrational quantum numbers referring to the excited electronic state and to the electronic ground state, respectively. $L_i(\tilde{\nu})$ is a normalized lineshape function for the i^{th} transition $|g0\rangle \rightarrow |ev_i^e\rangle$ with a typical FWHM width of the order of magnitude as a vibrational quantum. A calculation requires that the electronic transition moment is Taylor expanded in the nuclear coordinates. Due to the superposition of the intensity of the individual transitions in Eq. (11), it follows that the vibrational fine structure in UV/VIS absorption spectra of larger molecules is not well resolved as also experienced from experiments. This is different in the RADIS spectra, where the narrow Raman bands enable the excitation profiles to be well separated experimentally (as illustrated in **Figure 2**). Since each excitation profile only has contributions from a single Raman-active vibration, the vibrational fine structure in the UV/VIS absorption can be resolved. Thus, the amount of available information about the excited electronic molecular states is much larger in RADIS than in UV/VIS absorption.

It follows that while VRRS is mainly a vibrational spectroscopic technique, RADIS has more in common with electronic spectroscopy. It follows that each Raman-active vibration just plays the role of a “sensor” used to monitor the vibrational fine structure in the UV/VIS absorption spectrum.

Since the late 1980s, a very large amount of systematic resonance Raman studies on different metal complexes [28, 29] and different metal-porphyrins [12] including heme-proteins have been performed with the goal of determining their structure, their bio-functionality, and the conditions for aggregation. In these studies both the VRRS and RADIS including both excitation profiles and polarization dispersion have been applied. Recently polarization-resolved VRRS has been combined with dynamic light scattering to study among other things the aggregation of *Arenicola marina* extracellular hemoglobin, which is a macromolecule with 144 heme groups instead of four as in human hemoglobin [30]. As already mentioned one great advantage of applying Raman scattering is that the technique can be performed as reflection measurements without much sample preparation. Besides, the Raman signals can be obtained through glass and other sheets of protection. Thus, Raman studies can be performed as in vivo or in situ studies. We refer to the comprehensive Raman literature on these matters for details (e.g., see [31–36]). A complete RADIS experiment may be time-consuming or in some cases impossible to carry out due to the lack of excitation lasers with the proper wave number. It may also be time-consuming to determine the correct intensity variation when the excitation wave number is changed due to changes in the scattering conditions (laser intensity and focus, laser-induced degradation of the molecule, change of the fluorescence, etc.). The application of internal standards and other means have to be introduced in order to ensure the correct experimental conditions. However, in some cases of practical interest, it is in fact possible to extract valuable information without completing a full RADIS experiment (see Sections 4.2 and 4.3).

4. Examples

As has been shown, vibrational RS is exclusively a vibrational spectroscopic technique like IR and NIR. However, vibrational Raman spectroscopy performed under resonance conditions may be considered as either a vibrational spectroscopic technique or as an electronic spectroscopic technique, which of the two depends on the way the experiments are performed. Three examples are briefly discussed below. For more applications, the interested reader should consult the comprehensive Raman literature [31–36].

4.1 Example 1: perturbation of molecular symmetry

As demonstrated in [11], the non-commuting generator approach to molecular symmetry may be applied to calculate the structure of the state tensors. **Figure 3** shows an example for two vibrations in point group D_{4h} . The figure also demonstrates what happens when the symmetry is lowered so that the configuration is now described in point group D_{2h} . Lowering of the symmetry may be a result of a chemical reaction or may be due to a perturbation of the configuration from the planar square to a planar rectangular shape. To the left in the figure, the state tensors in D_{4h} for the Raman-active in-plane vibrations a_{1g} , a_{2g} , and b_{1g} are shown, which are written in front of the tensors. The symmetries of the two components of the resonating, degenerate electronic state with E_u symmetry are written in the tensors on the positions, which correspond to the only nonvanishing elements. The plus and minus signs describe the numerical relations between the tensor elements. For the a_{1g} vibration, it follows that $S_{xx}^{|e0=E_{u,x}\rangle} = S_{yy}^{|e0=E_{u,y}\rangle}$, while for the b_{1g} vibration, we have that $S_{xx}^{|e0=E_{u,x}\rangle} = -S_{yy}^{|e0=E_{u,y}\rangle}$. The state tensor for the a_{2g} vibration is antisymmetric, i.e., $S_{xy}^{|e0=E_{u,y}\rangle} = -S_{yx}^{|e0=E_{u,x}\rangle}$. From the tensor structure, the DPR values can be calculated by using Eq. (5) and the relations given in [11] or [3]. The DPR values are written to the right side of the tensors and are seen to be constants. By correlating the symmetries of the two point groups, the symmetries of the vibrations are changed as follows: $a_{1g} \rightarrow a_g$, $b_{1g} \rightarrow b_{2g}$ and $a_{2g} \rightarrow b_{g1}$. The state tensors for the a_g , b_{1g} and b_{g2} vibrations in D_{2h} are also shown in **Figure 3**. As before, inside the tensors the symmetries which the intermediate states must have in order

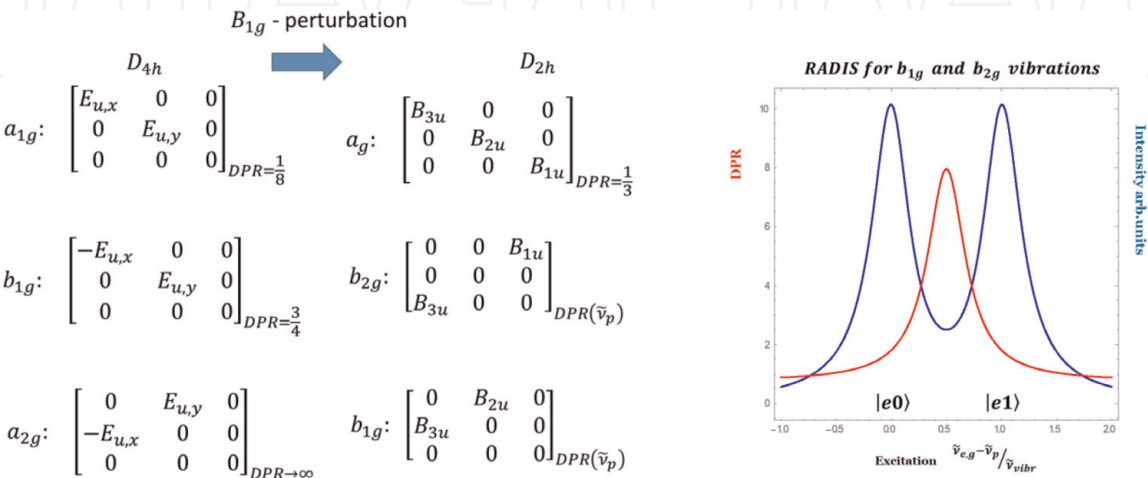


Figure 3.
(Left) Changes of the state tensors, induced by perturbation of a square planar (D_{4h}) molecular configuration into a rectangular planar (D_{2h}) configuration. (Right) Most notably is the change of the constant DPR into DPR dispersion (red curve) for the b_{1g}/b_{g2} vibrations (D_{2h}).

to give rise to any Raman signal are written. Due to the lowering of the symmetry, there are no longer numerical relations between the tensor components. Considering, e.g., the totally symmetric vibration, we see that a resonating state must have either B_{3u} , B_{2u} or B_{1u} symmetry and that, e.g., an electronic state with B_{3u} symmetry gives rise to a tensor where only $S_{xx}^{|e0=B_{3u}\rangle} \neq 0$.

For the asymmetric b_{2g} vibration, the B_{3u} electronic state would result in a tensor where only the component $S_{xx}^{|e0=B_{3u}\rangle} \neq 0$, whereas one vibrational excitation of this vibration gives a state with the symmetry $b_{2g} \otimes B_{3u} = B_{1u}$, which is seen to correspond to the transposed state tensor, i.e., only $S_{xz}^{|e1=B_{1u}\rangle} \neq 0$. From the power expansion of the vibronic state tensor given in Eq. (7), it may be shown that the two tensor elements satisfy the relation: $S_{xx}^{|e0\rangle} = S_{xz}^{|e1\rangle}$. A closer investigation shows that this relation is valid in general for asymmetric vibrations [11]. The Raman tensor is calculated by inserting the two state tensors in Eq. (3). The DPR is calculated by using Eq. (5) and the relations between the rotational invariants and the Raman tensor derived in [11]. By group theory, it can be shown that an external electronic perturbation with symmetry B_{1g} (in D_{4h}) would result in the considered shift in the molecular configuration. As shown in **Figure 3**, the consequence of the symmetry-lowering perturbation of the molecular configuration is that the DPR now shows a characteristic symmetric polarization dispersion with maximum half ways between the energy positions of the two states $|e0\rangle$ and $|e1\rangle$. The excitation profile is symmetric around the maximum of the DPR curve and has maxima at the positions of these states, i.e., at $|e0\rangle$ and $|e1\rangle$. In the point group D_{4h} , the state tensor for the a_{2g} vibration is purely antisymmetric with a result that the DPR becomes infinity. After the perturbation, where $a_{2g} \rightarrow b_{g1}$, the b_{1g} state tensor is seen to have the same structure as the tensor for the b_{2g} mode, which means that the DPR dispersion curve and excitation profile also become similar. However, the energy of the state $|e1\rangle$ will in general be different for different modes.

It follows that through the application of RADIS, it is possible to study small changes of the molecular configuration in excited electronic states and estimate the various molecular parameters influenced by these changes. As shown in numerous RRS papers on biomolecules, these structural changes, which are typically induced by minor changes in the environment of the molecule, can be studied in vivo, which is of course a major advantage [31–36].

4.2 Example 2: noninvasive color detection using polarization dispersion

The color of a molecular species is associated with the properties of the electronic excited states of the molecule, and in large biomolecules, it is due the presence of a chromophore being typically a metal complex. The red color of the heme-proteins, which is due to the presence of the Fe-porphyrin complex, is a well-known example. A change in color may be due to a change of the molecular configuration (distortion, aggregation) or be a result of a chemical reaction. By monitoring the color change before and after a chemical reaction, the substance concentration in solutions can be determined from the absorbance measured by a UV/VIS spectrophotometer or in the case of a solid by applying the spectrophotometer with an integrating sphere. In the literature several color detection methods have been developed for the detection of various substances. A book on color detection is in the process of publication by IntechOpen and will be published later in 2019.

In this section a reflection technique with high spectral resolution is discussed. The technique is suitable for the detection of minor color differences between

similar molecules, i.e., molecules where a number of identical vibrations can be identified in the vibrational signature of the molecules. The method has been applied in combination with polarized resolved fluorescence to study the stability of the Ruthenium-based dye N719 [37] and to study in vitro the stability of N719 and the adsorption and desorption processes of this complex to the TiO_2 substrate in dye-sensitized solar cells [38]. We refer to this paper for details.

Recently the method has also been proposed as a possible noninvasive screening technique for revealing a content of carbon monoxide in fresh tuna fish or meat. Preliminary experimental results were presented at the Raman conference ICORS 2016 in Brazil [39] and are discussed in the following.

The method is based on the presence of dispersive Raman modes combined with a small spectral difference between the visible absorption spectra of similar molecules. The idea is as follows: the resonance condition for a specific molecule in RRS depends, as we have seen above, on the difference in the wave number between the electronic absorption and the excitation laser. Due to the tensor property of resonance Raman scattering, the value of the DPR depends on this difference (polarization dispersion). Thus, a small spectral shift in the absorption will essentially be equivalent to a displacement of the polarization dispersion curve relative to the excitation wave number of the laser, as illustrated in **Figure 5**. The change of the DPR value at a specific wave number depends on the shape of the dispersion curve, which depends on the nature of the vibration and the Raman tensor. When the molecule has low or no symmetry, most Raman-active vibrations will be dispersive. Although the ideal symmetry of a chromophore is often high, which limits the number of dispersive modes, the real symmetry is frequently lowered due to perturbations of the chromophore, which opens up for dispersion. The heme group with the ideal symmetry D_{4h} is an example. This means that in reality the appearance of Raman modes exhibiting dispersion is quite common.

In the *modified atmosphere packaging* of fresh fish and meat products, the products are frequently exposed to carbon monoxide. Due to the higher binding affinity of CO in comparison with O_2 , CO replaces O_2 in myoglobin in the muscle tissue with high affinity, which results in the cherry-red carboxy-myoglobin complex MbCO. Due to the red color and high stability of MbCO, the fish or meat products will appear to be more fresh and attractive for a longer time period than the unexposed products. In [40] a quantitative method for the determination of CO bound to myoglobin based on visible absorption spectroscopy has been developed. Although this method has a high accuracy, it requires taking a sample from the product followed by sample preparation before the absorption spectra can be measured. **Figure 4** shows a fresh tuna beef sample together with the polarization-resolved RRS spectra measured on the sample without any sample preparation but measured before and after approximately 10 minutes of exposure to CO and exciting the sample with a solid-state 532 nm laser. The experimental DPR values estimated from six Raman modes are collected in **Figure 5**. Further experimental details including details on the data processing of the polarization-resolved RRS data are obtainable from the author. **Figure 5** also shows, as an example, a simulation of the DPR dispersion curves for the mode at 1450cm^{-1} present in the polarization-resolved RRS spectra and which has been assigned as a b_{1g} mode. The spectral shift (color shift) due to the exposure with CO is $\approx 9\text{nm}$ equivalent to 275cm^{-1} , estimated from measuring the diffuse reflectance of the tuna beef sample before and after exposure with CO with a Lambda 900 spectrophotometer equipped with an integrating sphere. The polarization-resolved RRS data were collected by using a fiber-coupled, 180° Raman microscope consisting of a modified Olympus BX60F5, a SpectraPro 2500i spectrograph (Acton) with 1200lines/mm

grating, cooled CCD (Princeton Instr/Acton PIXIS), and 532 nm cw laser (VentusLP532) focused with 10x objective with NA = 0.30. Collection optic: Same objective combined with Dichroic mirror and multimode fiber coupling to spectrograph. Av. integration time 30 seconds. No sample preparation.

First, it is noticed that the DPR values of five out the six modes indicate that they are dispersive, since all the DPR values are changed due to the exposure to CO. The polarization dispersion shows that the real symmetry of both MbO_2 and $MbCO$ must be lower than D_{4h} , which would give constant values for the DPR. It is also noticed that all the DPR values are smaller than 0.75, which indicate that the polarization dispersion is different from the one considered previously (see **Figure 3**). The DPR dispersion curve in **Figure 5** is calculated for the b_{1g} mode at 1450cm^{-1} . It is obtained by adopting the procedure discussed in [11], where instead of considering the exact symmetry of the perturbed molecule (e.g., D_{2h}) it is assumed that the molecule is really a weakly perturbed D_{4h} system. In our example it means that the state tensor relation $S_{xx}^{e0=E_u,x} = -S_{yy}^{e0=E_u,y}$ is still valid, but the degeneracy of the $|E_u\rangle$ state is lifted because of the perturbation, so that the two contributions to the Raman tensor now appear at slightly different energies (wave numbers). The splitting of the energy of the $|E_u\rangle$ state combined with the relation between the state tensors gives rise to constructive and destructive interference

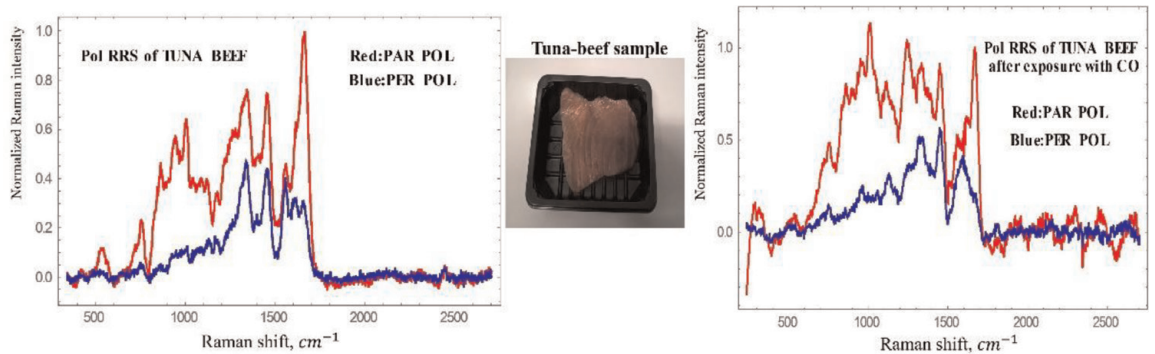


Figure 4. Fluorescence-corrected and normalized polarization-resolved RRS spectra of the tuna beef sample measured before and after 10 minutes. Exposure with CO.

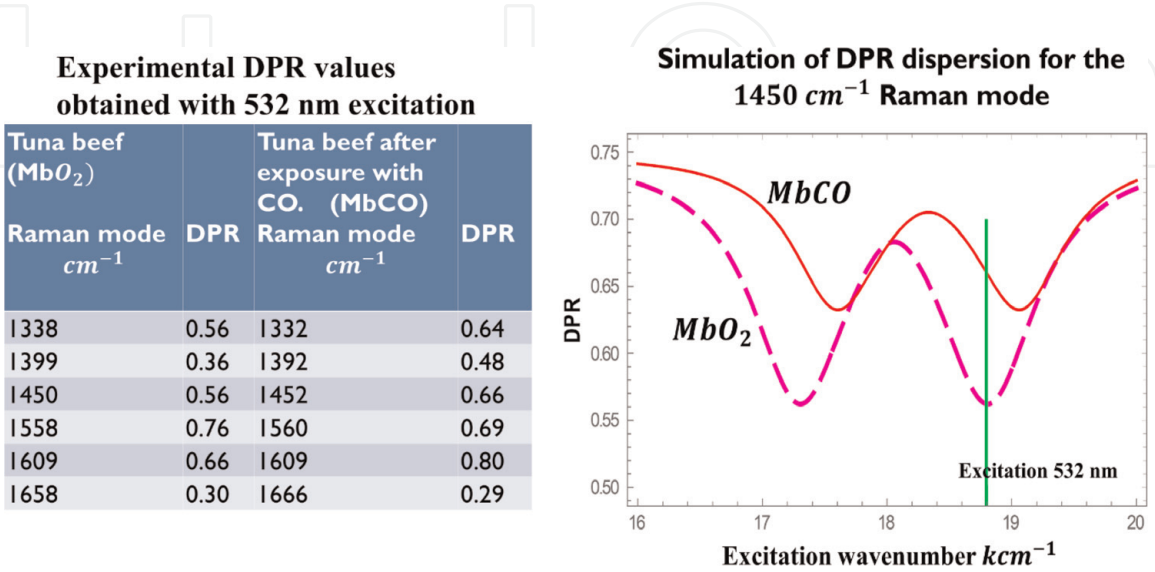


Figure 5. Left: experimental DPR determined from the polarized RRS data in **Figure 4** using a 6 mode fit (details available from author). Right: simulation and best fit of the DPR dispersion for the b_{1g} mode at 1450cm^{-1} applying an “electronic interference model.”

phenomena in the Raman intensities in the resonance region. Each dispersion curve in **Figure 5** is calculated by using only a single adjustable parameter, namely, the energy splitting of the $|E_u\rangle$ state. The energy splittings, which give the best fit to the experimental values, are as follows: 465cm^{-1} and 330cm^{-1} for MbO_2 and MbCO , respectively. The energy splittings are small in comparison with the vibrational wave numbers and correspond therefore to a small perturbation of the molecules away from the D_{4h} configuration. Since the small energy splittings are also comparable to the estimated bandwidths of the electronic transitions ($\gamma_{|E_u\rangle} \sim 400\text{cm}^{-1}$), they are not resolved in the visible absorption spectra, but as it follows from **Figure 5**, they give rise to measurable effects in the DPR dispersion. At the excitation wave number $18,797\text{cm}^{-1}$ corresponding to excitation with the 532 nm laser, the change of the DPR value, induced by the exposure with CO, is about 10%. The outcome of the experiment can be improved when the DPR data from all dispersive modes is considered. Another improvement, which would increase the reliability of the results considerably, would be a simultaneous measurement of the parallel and perpendicular polarized spectra, since this opens up for randomization and spatial averaging of the data. Simultaneous measurements of both polarizations can be obtained by modifying the excitation and collection optics in a standard Raman setup with CCD detector, in such a way that the upper and lower halves of the CCD can collect the parallel and perpendicular polarized spectra, respectively. This modification would also permit applications of polarization-resolved Raman imaging.

4.3 Example 3: unpolarized RADIS as a source of three-way multivariate data

In the last decade, chemometrics has become essential in the analysis of small differences of the chemical composition of samples in medical and environmental applications as well as in the food industry. Typically the chemical data are generated by different kinds of molecular spectroscopy: UV/VIS, fluorescence, NIR, IR, Raman, and others. A large number of mathematical methods have been developed and are in most cases part of the software package delivered with the spectrometer. The data from spectroscopy are in most cases two-way data set. Using vibrational Raman spectroscopy as an example, the elements x_{ik} in the data matrix are as follows: $x_{ik} = I_{\text{Raman}}^{(i)}(\tilde{\nu}_k)$, i.e., the Raman intensity at the wave number point $\tilde{\nu}_k$ in the Raman spectrum for the i^{th} sample. Typically, these data are analyzed by the application of principal component analysis (PCA). Despite the fact that PCA analysis often gives reliable results in chemical classification problems, the recent analysis of biological samples shows that in order to obtain sufficiently high recognition ratio for secure diagnostics, one has to work with very large data sets. One way is to work with three-way data, which in general has higher information density, instead of two-way data and then apply an appropriate three-way multivariate algorithm. In classification problems involving biological samples, the three-way data has been produced by combining UV/VIS absorption data with fluorescence data in the following way: the UV/VIS absorption is measured at selected wave numbers, and the fluorescence generated at these wave numbers is measured as well. Due to low spectral resolution in both these kinds of spectra, one must produce a data matrix with very high dimension, which has the consequence that a very large number of samples must be available.

In [41] a new application of RADIS has been proposed, where the coherent absorption-emission property of Raman scattering is utilized. When we compare the construction of three-way data by combining UV/VIS and fluorescence data with the RADIS in **Figure 2**, we see that the unpolarized RADIS data must

automatically be born as three-way data and more importantly the spectral resolution is very high. Consequently, only few data points along the Raman shift axis $\tilde{\nu}_k$ and along the excitation axis $\tilde{\nu}_j$ ($\tilde{\nu}_j$ is an excitation wave number) for small number of samples are really needed. Thus, the elements of the RADIS data matrix are given as $x_{ijk} = I_{Raman}^{(i)}(\tilde{\nu}_j, \tilde{\nu}_k)$. In [41] the RADIS data matrix has been analyzed by the application of a Tucker3 multivariate model, and various classification problems have been simulated and studied with the result that only few samples (<10) and few Raman lines (3–4) and few excitation wave numbers (2–3) are needed to obtain reliable results. We refer to [41] for details.

5. Conclusions

What is vibrational Raman spectroscopy: a vibrational or an electronic spectroscopic technique or both? Although the Raman signal reflects the vibrational motions of the molecule in the electronic ground state, our discussion shows that the answer to the question is that the Raman technique can be applied both as a vibrational and as an electronic spectroscopic technique depending on the experimental conditions chosen.

The Raman signal provides a highly resolved vibrational signature of the molecule. However, the signature depends on whether the molecular system (molecule or ion) is excited in non-resonance or in resonance with an electronic transition. In non-resonance it follows from Eqs. (9) to (10) that the Raman signal depends on the molecular polarizability tensor evaluated in the electronic ground state and not on the molecular dipole moment as in IR and NIR. In principle all fundamental vibrations in the molecule, where $\left(\frac{\partial \hat{\alpha}_{\rho\sigma}}{\partial Q_k}\right)_0 \neq 0$, may contribute to the vibrational signature. The excited electronic states have no influence on the vibrational signature. The non-resonance Raman technique is therefore a genuine vibrational technique similar to IR and NIR. The main differences are that the Raman signals are measured in a different way than the IR and NIR signals and that the polarization may, for smaller and symmetric molecules, provide additional information, also for solutions.

In resonance, where the laser wave number is chosen within an electronic absorption band of the molecule, Eq. (3) shows that the state tensors being closest to resonance with the laser will contribute most to the Raman tensor and to the Raman signal (resonance enhancement). Thus, the vibrations appearing in the resonance Raman spectra are mainly those associated with the electronic absorption. As discussed in Sections 3.2 and 3.3 and illustrated in **Figure 2**, resonance Raman scattering may form the basis of two different kinds of resonance Raman techniques termed VRRS and RADIS. In VRRS the focus is on the vibrational Raman spectra, just like in RS, but now obtained under resonance conditions, while in RADIS the focus is on the excitation profiles and the polarization dispersion curves. In RADIS the total Raman signal and the polarization-resolved Raman signals (giving the DPR defined in Eq. (5)) for a specific Raman-active vibration are monitored as a function of the excitation wave number. The vibronic expansion of the state tensor given in Eq. (7) shows that the Raman signal in resonance is determined by the electronic transition moment of the resonating state and its derivatives and by the relations between the vibrational sub-states associated with the electronic ground state (i.e., $|v_a\rangle$ and $|v_b\rangle$) and the resonating electronic states (i.e., $|v_e\rangle$). Since this will change the selection rules as compared to non-resonance, the vibrational signature of a specific molecule obtained from VRRS is therefore generally different

from the signature obtained from RS, and it depends on the specific wave number of the laser. Due to appearance of overtones and combination bands in the VRRS, the anharmonic corrections to the vibrational potential function in the electronic ground state can be estimated. It follows that VRRS is a vibrational spectroscopic technique, where the properties of the resonating states and the state tensors associated with these have an important influence on the spectral distribution.

Since the VRRS technique can be applied also as time-resolved spectroscopy, it is an attractive tool for the investigation of both the structure and dynamics of biomolecules. The main advantage of VRRS is the ability to investigate different parts of a large protein molecule by tuning the excitation wave number into the absorption band of the chromophore of interest. In a recent paper [42], the application of VRRS in the study of the structure and dynamics of various proteins is discussed. [42] gives an excellent review of this field covering both visible and UV resonance Raman as well as cw and time-resolved versions of VRRS.

The polarization properties of the resonance Raman signal are more important in resonance than in non-resonance. For example, as discussed in [43], the uniqueness of the polarization-resolved VRRS spectra combined with standard PCA chemometrics enables one to discriminate between closely related biomolecules with almost identical unpolarized VRRS spectra. The key point is that structural molecular change manifests itself through a change of the polarization of the Raman signal (DPR). The DPR defined in Eqs. (4) and (5) is an absolute quantity, which in combination with standard PCA renders the multivariate analysis insensitive to sample and experimental variations.

The discussion in Section 3.3 and the examples presented in Section 4 demonstrate that RADIS is closer to UV/visible absorption spectroscopy than it is to vibrational spectroscopy. Besides the spectral resolution is much higher enabling the vibrational fine structure of the absorption spectra to be resolved. In resonance, the interference between the state tensors, which is the origin of the sensitivity of the Raman signal with respect to changes of the molecular parameters, is restricted to those with energy denominators closest to the laser wave number. It was also demonstrated that the polarization properties of the Raman signal, expressed through the DPR, play a more important role than in non-resonance. As said already, the DPR is defined as the ratio between two Raman signals with different polarization. The interference, which can be both constructive and destructive, will in general be different in the two Raman signals depending on the wave number of the laser and the structure of the state tensors, which again is determined by the molecular symmetry and physical properties of the molecule. Section 4.1 and **Figure 3** illustrate a simple example, where the molecular configuration in an electronically excited state is distorted, which, as seen, creates a significant polarization dispersion. To fully exploit the sensitivity of the DPR to changes in the molecular parameters, one must determine the polarization dispersion, i.e., one must monitor two resonance Raman spectra (the parallel and perpendicular polarized) at each laser wave number available. Traditionally the Raman spectra with different polarizations are measured in sequence. However, with CCD technology it is possible to measure the two Raman signals simultaneously, which will improve the accuracy of the DPR considerably. This requires a modification of the entrance and collection optics of a standard Raman spectrometer, so that the upper and lower halves of the CCD monitor the parallel and perpendicular polarized Raman signals, respectively [44, 45].

The examples discussed in Section 4.2 show that it is possible to detect a small change in color of a molecular sample by determining the change of the DPR of a dispersive Raman mode, applying only a single excitation wave number in the absorption spectrum. To be detected the color change must be due to a modification

of the chromophore, so that the same Raman modes are present before and after the color change. Also in these examples, the resonance Raman technique performs as a kind of electronic technique.

Finally, it is shown in Section 4.3 that due to the coherent nature of the Raman process it generates automatically the so-called three-way multivariate data. This property is applied to solve chemical classification problems by using only a few (2–3) excitation wave numbers in un-polarized RADIS in combination with a three-way multivariate model. As shown, only very few samples (<10) are needed, instead of the very large (500–600) number of samples required, when the visible absorption and fluorescence spectra are combined to produce the three-way data.


Author details

Søren Hassing

Institute of Chemical Engineering, Biotechnology and Environmental Technology,
University of Southern Denmark, Odense, Denmark

*Address all correspondence to: sh@kbm.sdu.dk

IntechOpen

© 2019 The Author(s). Licensee IntechOpen. This chapter is distributed under the terms of the Creative Commons Attribution License (<http://creativecommons.org/licenses/by/3.0>), which permits unrestricted use, distribution, and reproduction in any medium, provided the original work is properly cited. 

References

- [1] Raman CV, Krishnan KS. A new type of secondary radiation. *Nature*. 1928; **121**:501
- [2] Raman CV. A new radiation. *Indian Journal of Physics*. 1928;**2**:387-398
- [3] Long DA. *The Raman Effect*. Chichester: John Wiley & Sons; 2002. ISBN: 978-0-471-49028-9
- [4] Gordon JP, Zeiger HJ, Townes CH. The maser-new type of microwave amplifier, frequency standard and spectrometer. *Physics Review*. 1955;**99**: 1264-1274
- [5] Schawlow AL, Townes CH. Infrared and optical masers. *Physics Review*. 1958;**112**:1940
- [6] Boyle WS, Smith GE. Charge-coupled semiconductor devices. *Bell System Technical Journal*. 1970;**49**: 487-493
- [7] Smith BA. Astronomical imaging applications for CCDs. In: JPL Conference on Charge-Coupled Device Technology and Applications; 1976. pp. 1235-1238
- [8] Xie L, Ling X, Fang Y, Zhang J, Liu Z. Graphene as a substrate to suppress fluorescence in resonance Raman spectroscopy. *Journal of the American Chemical Society*. 2009;**131**(29): 9890-9891
- [9] Placzek G. In: Marx E, editor. *Handbuch der Radiologie*. Vol. 2. Leipzig: Akademische Verlagsgesellschaft; 1934. pp. 209-374
- [10] Long DA. *Raman Spectroscopy*. London, UK: McGraw Hill; 1977
- [11] Mortensen OS, Hassing S. Chapter 1: Polarization and interference phenomena in resonance Raman scattering. In: Clarke RJH, Hester RE, editors. *Advances in Infrared and Raman Spectroscopy*. Vol. 6. New York (US): Wiley; 1980
- [12] Schweitzer-Stenner R. Polarized resonance Raman dispersion spectroscopy on metallocporphyrins. *Journal of Porphyrins and Phthalocyanines*. 2001;**5**(3):198-224. DOI: 10.1002/jpp.307
- [13] Siebrand W, Zgierski MZ. In: Lim C, editor. *Excited States*. Vol. 4. New York: Academic Press Inc.; 1979. pp. 1-134
- [14] Kramers HA, Heisenberg W. Über die Streuung von Strahlung durch Atome. *Zeitschrift für Physik*. 1925; **31**(1):681-708
- [15] Weisskopf V. Zur Theorie der Resonanzfluoreszenz. *Annals of Physics*. 1931;**9**:23
- [16] Goldberger KM, Watson KM. *Collision Theory*. New York, US: Dover Books on Physics; 2004. p. 944. ISBN-13: 978-0486435077
- [17] Davydov AS. *Quantum Mechanics*. 1st ed. Oxford: Pergamon Press; 1965. p. 680
- [18] Dirac PAM. *The Principles of Quantum Mechanics*. 4th ed. Clarendon Press: Oxford; 1967. 314p
- [19] Mortensen OS. *Structure and Bonding*. Vol. 69. Berlin Heidelberg, Germany: Springer-Verlag; 1987. pp. 1-38
- [20] Hassing S. In: Khan M, editor. *Raman Spectroscopy and Applications*. Rijeka, Croatia: InTech; 2017. pp. 143-162
- [21] Spiro TG, Strekas TC. Resonance Raman spectra of hemoglobin and cytochrome c: Inverse polarization and

- vibronic scattering. Proceedings of the National Academy of Sciences of the United States of America. 1972;**69**: 2622-2626
- [22] Shelnutt JA, Cheung LD, Chang RCC, Yu N, Felton LH. Resonance Raman spectra of metalloporphyrins. Effects of Jahn-Teller instability and nuclear distortion on excitation profiles of Stokes fundamentals. The Journal of Chemical Physics. 1977;**66**:3387-3398
- [23] Shelnutt JA, O'Shea DC. Resonance Raman spectra of copper tetraphenylporphyrin: Effects of strong vibronic coupling on excitation profiles and the absorption spectrum. The Journal of Chemical Physics. 1978;**69**: 5361-5374
- [24] Zgierski MZ, Pawlikowski M. Depolarization dispersion curves of resonance Raman fundamentals of metalloporphyrins and metallophthalocyanines subject to asymmetric perturbations. Chemical Physics. 1982;**65**:335-367
- [25] Siebrand W, Zgierski MZ. Effect of solvent-induced line broadening on resonance Raman excitation profiles and depolarization ratios. The Journal of Physical Chemistry. 1982;**86**(24): 4718-4725
- [26] Mortensen OS. Polarization dispersion in resonance Raman scattering. The effect of inhomogeneous broadening. Chemical Physics Letters. 1976;**43**(3):576-580
- [27] Albrecht AC. On the theory of Raman intensities. The Journal of Chemical Physics. 1961;**34**:1476-1484
- [28] Waage Jensen P, Jørgensen Bonne L. Resonance Raman spectroscopy of some iron(II) imine complexes. Journal of Molecular Structure. 1982;**79**:71-78
- [29] Waaben Hansen P, Waage Jensen P. Vibrational studies on bisd-terpyridine-ruthenium(II) complexes. Spectrochimica Acta A. 1994;**50**:169-183
- [30] Jernshøj KD, Hassing S, Olsen LF. A combination of dynamic light scattering and polarized resonance Raman scattering applied in the study of Arenicola Marina extracellular hemoglobin. The Journal of Chemical Physics. 2013;**139**(6):065104
- [31] Lemke C, Dreybrodt W, Shelnutt J, Quirke JME, Schweitzer-Stenner R. Polarized Raman dispersion spectroscopy probes planar and non-planar distortions of Ni(II)-porphyrins with different peripheral substituents. Journal of Raman Spectroscopy. 1998;**29**: 945-953
- [32] Guthmuller J, Champagne B. Simulating and interpreting vibrational spectra of molecules: The resonant Raman spectra of rhodamine 6G. In: AIP Conference Proceedings; 2012. 1504, p. 928. doi: 10.1063/1.4771848
- [33] Kiewisch K, Neugebauer J, Reiher M. Selective calculation of high-intensity vibrations in molecular resonance Raman spectra. The Journal of Chemical Physics. 2008;**129**:204103. DOI: 10.1063/1.3013351
- [34] Wächtler M, Guthmuller J, Gonzalez L, Dietzek B. Analysis and characterization of coordination compounds by resonance Raman spectroscopy. Coordination Chemistry Reviews. 2012;**256**:1479-1508. DOI: 10.1016/j.ccr.2012.02.004
- [35] Jentzen M, Ma J, Shelnutt JA. Conservation of the conformation of the porphyrin macrocycle in hemoproteins. Biophysical Journal. 1998;**74**:753-763
- [36] Schindler J, Kupfer S, Ryan AA, Flanagan KJ, Senge MD, Dietzek B. Sterically induced distortions of nickel (II) porphyrins—Comprehensive investigation by DFT calculations and resonance Raman spectroscopy.

- Coordination Chemistry Reviews. 2018; **360**:1-16. DOI: 10.1016/j.ccr.2017.12.014
- [37] Hassing S, Jernshøj KD, Nguyen PT, Lund T. Investigation of the stability of the ruthenium-based dye (N719) utilizing the polarization properties of dispersive Raman modes and/or of the fluorescent emission. *Journal of Physical Chemistry C*. 2013;**117**:23500-23506
- [38] Hassing S, Jernshøj KD, Nguyen PT, Lund T. In vitro polarized resonance Raman study of N719 and N719-TBP in dye sensitized solar cells. *Journal of Technology Innovations in Renewable Energy*. 2016;**5**:21-32
- [39] Hassing S. Non-invasive determination of the CO contents in tuna fish using polarization resolved resonance Raman and/or Rayleigh spectroscopy. In: Program of XXV 2016 ICORS; Brazil; Abstract p. 61. Conference paper presented available upon request from sh@kbm.sdu.dk
- [40] Smulevich G, Droghetti E, Focardi C, Coletta M, Ciaccio C, Nocentini M. A rapid spectroscopic method to detect the fraudulent treatment of tuna fish with carbon monoxide. *Food Chemistry*. 2007;**101**:1071-1077
- [41] Hedegaard M, Hassing S. Application of Raman dispersion spectroscopy in 3-way multivariate data analysis. *Journal of Raman Spectroscopy*. 2007;**39**:478-489
- [42] López-Peña I, Leigh BS, Schlamadinger DE, Kim JE. Insights into protein structure and dynamics by ultraviolet and visible resonance Raman spectroscopy. *Biochemistry*. 2015; **54**(31):4770-4783. DOI: 10.1021/acs.biochem.5b00514
- [43] Hassing S, Jernshøj KD, Hedegaard M. Solving chemical classification problems using polarized Raman data. *Journal of Raman Spectroscopy*. 2011;**42**: 21-35
- [44] Kerdoncuff H, Pollard MR, Westergaard PG, Petersen JC, Lassen M. Compact and versatile laser system for polarization-sensitive stimulated Raman spectroscopy. *Optics Express*. 2017; **25**(5):5618-5625. DOI: 10.1364/OE.25.005618
- [45] Kiefer J. Simultaneous acquisition of the polarized and depolarized Raman signal with a single detector. *Analytical Chemistry*. 2017;**89**:5725-5728. DOI: 10.1021/acs.analchem.7b01106